Article

Disentangling Sum-Frequency Generation Spectra of the Water Bending Mode at Charged Aqueous Interfaces

Published as part of The Journal of Physical Chemistry virtual special issue "Yoshitaka Tanimura Festschrift".

Takakazu Seki,[#] Chun-Chieh Yu,[#] Kuo-Yang Chiang, Junjun Tan, Shumei Sun, Shuji Ye, Mischa Bonn, and Yuki Nagata*
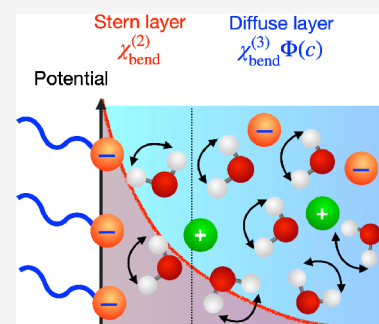
Read Online

ACCESS | Metrics & More | Article Recommendations | Supporting Information

ABSTRACT: The origin of the sum-frequency generation (SFG) signal of the water bending mode has been controversially debated in the past decade. Unveiling the origin of the signal is essential, because different assignments lead to different views on the molecular structure of interfacial water. Here, we combine collinear heterodyne-detected SFG spectroscopy at the water-charged lipid interfaces with systematic variation of the salt concentration. The results show that the bending mode response is of a dipolar, rather than a quadrupolar, nature and allows us to disentangle the response of water in the Stern and the diffuse layers. While the diffuse layer response is identical for the oppositely charged surfaces, the Stern layer responses reflect interfacial hydrogen bonding. Our findings thus corroborate that the water bending mode signal is a suitable probe for the structure of interfacial water.

I. INTRODUCTION

The bending mode of H$_2$O has a characteristic frequency around 1550−1700 cm^{-1}. This mode has been probed using vibrational spectroscopies, because it reports on the local structure of the hydrogen-bond network in water; when water is strongly (weakly) hydrogen-bonded, the frequency of the bending mode is blue-shifted (red-shifted).[1,2] Probing the bending mode of water has several advantages over probing the O−H stretch mode. Whereas the O−H stretch mode of water cannot be spectrally distinguished from other molecules containing OH-groups, the H−O−H water bending mode is specific to water.[3−8] Also, the vibrational coupling between bending modes has a limited impact on its spectral response,[3,9] in sharp contrast to the O−H stretch mode.[10,11] Furthermore, understanding the bending mode is essential to unveil the vibrational energy transfer from the O−H stretch mode of water and the amide mode of proteins to the local heat,[12−16] because the bending mode is believed to be an essential intermediate step to receive excess vibrational energy and release it to the local heat.[9,17−21]

The H−O−H bending mode of specifically interfacial water molecules has been probed with sum-frequency generation (SFG) spectroscopy.[3,22−28] Although SFG spectroscopy is surface-specific, the precise origin of the SFG signal has been highly debated. So far, three distinct contributions have been proposed, from interfacial dipoles, bulk quadrupoles, and interfacial quadrupoles.[29,30] The dipole contribution refers to the first-order term of the second-order susceptibility, and a number of research groups have analyzed and interpreted the experimental and simulated SFG data of the bending mode

based on the dipole mechanism.[22−24,31−33] The bulk quadrupole mechanism was proposed by Tahara, Morita, and co-workers in 2016, in which the first-order dipole term is masked by a higher-order term.[27] More recently, in 2020, a new set of the bending mode SFG spectra demonstrated the frequency shift of the bending mode due to the interaction of water with lipids/surfactants. Because the frequency shift cannot be accounted for via the bulk quadrupole mechanism, Tahara and co-workers proposed that the bending mode SFG signal is generated by the higher-order term arising from the interface (interfacial quadrupole mechanism).[28]

Clarifying this apparent contradiction by unveiling the origin of the SFG signal is important, because the different assignments of the origin of the signal lead to different interpretations of the bending mode of water—and thereby of the structure of interfacial water. If the $\chi^{(2)}_{bend}$ signal arises from the dipole mechanism, it provides information on the molecular orientation of the interfacial water molecules.[34] If the signal arises through the interfacial quadrupole mechanism, one cannot obtain orientational information.[35,36]
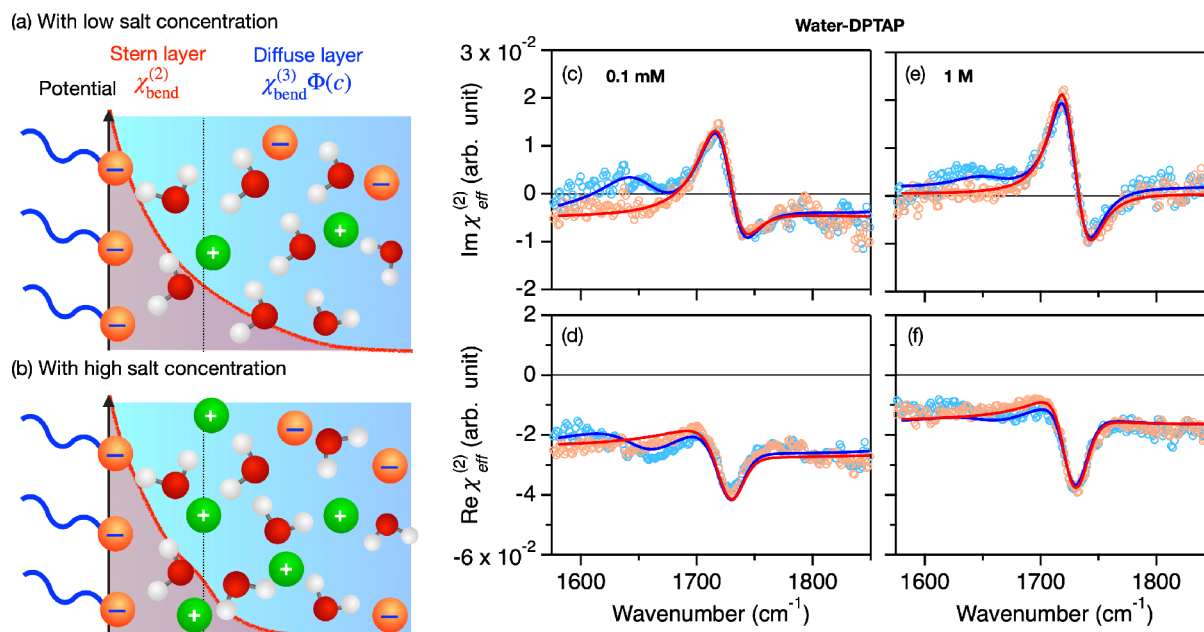
Currently, the bulk quadrupole mechanism is not supported by any experimental data. The remaining two mechanisms,

Figure 1. (a,b) Schematics for the Stern layer and the diffuse layer contributions corresponding the $\chi^{(2)}_{bend}$ and $\chi^{(3)}_{bend}(\omega)\Phi(c)$ contributions, respectively, in the presence of (a) low concentration and (b) high concentration of salt. $\Phi(c)$ represents the surface potential as a function of salt concentration. (c–f) HD-SFG spectra at the H_2O−DPTAP interface and at the D_2O−DPTAP interface with two different NaCl concentrations. The blue and red data points indicate the H_2O−DPTAP and D_2O−DPTAP data, respectively. The solids lines represent the fits.

dipole mechanism and interfacial quadrupole mechanism, can be identified from the sign of the H−O−H bending mode ($\chi^{(2)}_{bend}$) at the charged interfaces. If $\chi^{(2)}_{bend}$ is governed by the dipole mechanism, the sign of the $Im(\chi^{(2)}_{bend})$ signal changes with the sign of the surface charge. If $\chi^{(2)}_{bend}$ is governed by the interfacial quadrupole mechanism, the sign of the $Im(\chi^{(2)}_{bend})$ signal is positive, irrespective of the sign of the surface charge.[36]

Extracting the $\chi^{(2)}_{bend}$ contribution at the charged interfaces is, however, not straightforward because the water signal at these interfaces arises not only from the oriented water molecules in the Stern layer ($\chi^{(2)}_{bend}$ term) which is invariant to the solution's salt concentration, but also from those oriented along the interfacial electric field in the diffuse layer ($\chi^{(3)}_{bend}$ term) (Figure 1a,b).[37] This interfacial field and the magnitude of the $\chi^{(3)}_{bend}$ contribution has been examined by varying the bulk electrolyte concentration.[38−40] However, the $\chi^{(3)}_{bend}$ contribution is controversial: Reference 26 indicated a substantial $\chi^{(3)}_{bend}$ contribution, leading to the flipping of the sign of the $Im(\chi^{(2)}_{bend})$ peak due to the change of the negatively and positively charged interfaces (dipole mechanism), while ref 28 showed that the $\chi^{(3)}_{bend}$ contribution is negligible, leading to the positive $Im(\chi^{(2)}_{bend})$ peak irrespective of negatively or positively charged interfaces (interfacial quadrupole mechanism).

Here, using collinear heterodyne (HD)-SFG, we measure the H−O−H bending mode of water at the positively charged lipid (1,2-dipalmitoyl-3-trimethylammonium propane, DPTAP) and negatively charged lipid (1,2-dipalmitoylsn-glycero-3-phospho-glycerol, DPPG) interfaces. We unambiguously establish that the $\chi^{(3)}_{bend}$ contribution is non-negligible and determine its spectrum. The careful extraction of the $Im(\chi^{(2)}_{bend})$ signal, by varying the electrolyte concentration, reveals that the sign of the $Im(\chi^{(2)}_{bend})$ signal is opposite at the water−DPTAP and water−DPPG interfaces. We highlight the importance of the homogeneous sampling of the water−lipid interface, which
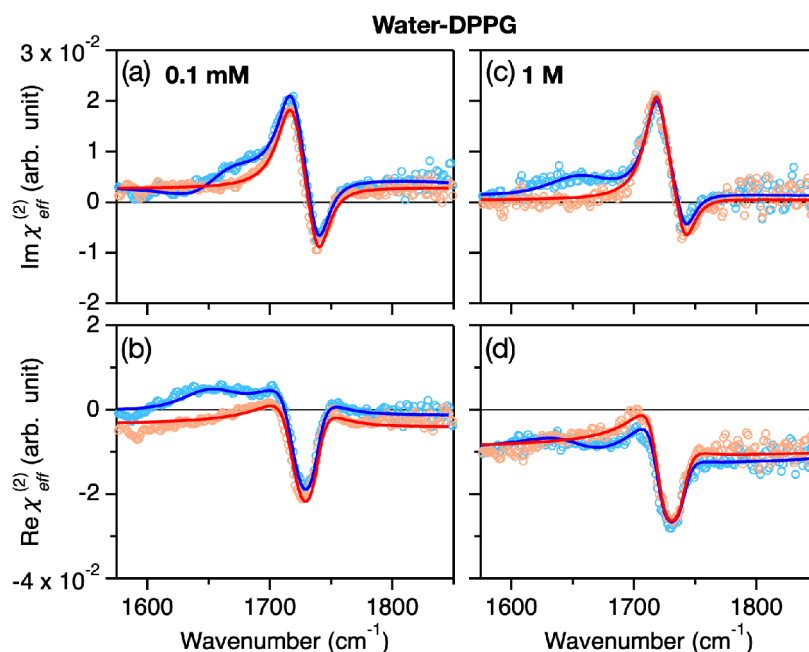
could be achieved by rotating the sample in the collinear HD-SFG setup.

II. METHODS

II.A. Sample Preparation. We dissolved DPPG (sodium salt) and DPTAP (chloride salt) purchased from Avanti Polar Lipids in a mixture of 90% chloroform (Fischer Scientific, stabilized with amylene, >99%) and 10% methanol (VWR Chemicals, 99.8%) at a concentration of 4.3×10^{-4} mol/L. Sodium chloride (Sigma-Aldrich, >99.5%) was baked in an oven for 8 h at 650 °C. We used D_2O (>99.9%), which was purchased from Sigma-Aldrich. H_2O was obtained from a Milli-Q machine (resistance >18.2 MΩ cm). We prepared the sodium chloride solutions with their concentrations of 1 M and 0.1 mM. We chose the concentrations of 0.1 mM and 1 M to see the spectral deformations in both imaginary and real parts due to the complex $\chi^{(3)}_{bend}$ term, as is seen in what follows.

The 20 mL sodium chloride solutions were poured into a Teflon trough with an 8.0 cm diameter. We then deposited ~50 μL DPTAP and DPPG solutions onto the H_2O and D_2O solutions using a click syringe. The surface pressure of the DPTAP and DPPG monolayers was measured with a commercial surface tension meter (Kibron, Inc., Helsinki, Finland) and was determined to be ~44 ± 3 mN/m and 19 ± 3 mN/m, respectively. The surface area per lipid was estimated to be ~44 Å² and ~52 Å² for DPTAP and DPPG, respectively.[41,42] The prepared samples were equilibrated for at least 40 min. For both HD-SFG and HD-SHG measurements, the trough was rotated to avoid the lipid monolayer distortion due to heat accumulation.[43] The speed of the sample at the laser irradiation spot was ~1.0 cm/s.

In this study, we used the charged lipids of DPPG and DPTAP with the C═O groups. The C═O stretch mode contributions interfere with the H−O−H bending mode of water,[26] which may potentially complicate the interpretation on the SFG spectra. The other choices which have been

Figure 2. (a–d) HD-SFG spectra at the H_2O–DPPG and D_2O–DPPG interfaces with two different NaCl concentrations. The blue and red data points indicate H_2O–DPPG and D_2O–DPPG data, respectively. The solids lines represent the fits.

commonly used for generating the charged surfaces are the surfactants without the C=O groups, such as sodium dodecyl sulfate (SDS) and cetyltrimethylammonium bromide (CTAB).[24,44] However, SDS and CTAB have critical micellar concentrations of ~0.1 mM to 1 mM, much higher than DPPG and DPTAP. In fact, for stable SFG measurements, researchers have used 1 mM–10 mM concentrations of SDS and CTAB.[44–46] Such high SDS and CTAB bulk concentrations prohibit fine control of charge screening by sodium chloride to tune the $\chi_{bend}^{(3)}$ contribution, which requires concentrations down to 0.1 mM. The bulk concentrations of the DPPG and DPTAP samples were ~1 μM, much smaller than the 0.1 mM salt concentration. For DPPG and DPTAP, one can control the ionic strength with the salt concentration, allowing us to uncover the $\chi_{bend}^{(3)}$ contribution, unlike SDS and CTAB.

II.B. HD-SFG Measurements. The HD-SFG measurements were performed on a collinear beam geometry using a Ti:Sapphire regenerative amplifier (Spitfire Ace, Spectra-Physics, centered at 800 nm, ~40 fs pulse duration, 5 mJ pulse energy, 1 kHz repetition rate). The visible and IR beams were first focused into a 20 μm-thick y-cut quartz plate to produce sum-frequency signal serving as local oscillator (LO). These beams were then collinearly passed through an 8 mm CaF_2 plate for the phase modulation and focused on the sample surface at an angle of 45°. The SFG signal from the sample interferes with the SFG signal from the LO, generating the SFG interferogram. The SFG interferogram was dispersed in a spectrometer and detected by an EMCCD camera. The complex $\chi_{eff}^{(2)}$ spectra were obtained via the Fourier analysis of the interferogram and normalization by a z-cut quartz crystal. The measurements were performed with *ssp* (denoting *s-*, *s-*, and *p*-polarized SFG, visible, and IR beams, respectively) polarization combination. The details of the HD-SFG setup can be found in the Supporting Information.
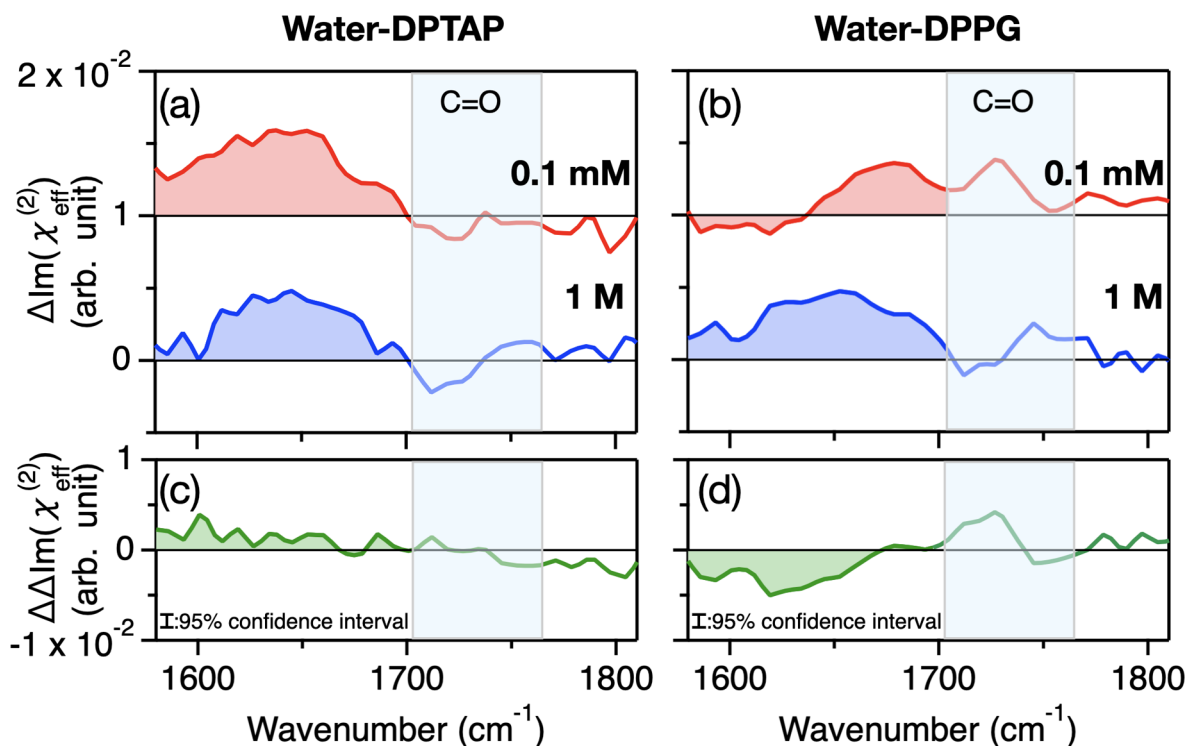
Note that the HD-SFG measurement for the rotating sample is challenging because the height of the sample fluctuates due to the rotation of the sample, causing phase modulations. The

height fluctuation of our samples had a standard deviation of 1.7 μm, which will cause ~6° phase error with a typical noncollinear SFG setup.[47] In this work, we used a collinear HD-SFG geometry, which is much less sensitive to the height change than the noncollinear HD-SFG setup, and thus the phase error for the rotating sample is <1.7°.[48–50] Such a collinear HD-SFG setup is thus very suitable for HD-SFG measurements of rotating samples.

II.C. HD-SHG Measurements. A pulsed Yb:KGW (ytterbium-doped potassium gadolinium tungstate) laser system (Pharos, Light Conversion Ltd.) was used, generating pulses with a wavelength of ~1030 nm, a pulse duration of roughly 210 fs, a repetition rate of 1 MHz, and a pulse energy of 15 μJ. The pulse energy was reduced to 300 nJ. After passing through y-cut quartz to generate the LO signal, and fused silica plates for phase modulation, the fundamental beam was focused onto the sample surface. All the measurements were performed with *s-in/p-out* polarization combinations. The incident angle of the incoming beam was set to 45° relative to the surface normal. The generated second harmonic generation (SHG) signal was dispersed in a spectrograph and detected by an EMCCD camera.

III. RESULTS AND DISCUSSION

III.A. Evidence of Non-negligible $\chi_{bend}^{(3)}$ Contribution. Figures 1c,f display the complex SFG susceptibility ($\chi_{eff}^{(2)}$) at the D_2O–DPTAP and H_2O–DPTAP interfaces with two different salt concentrations. First, we focus on the Im($\chi_{eff}^{(2)}$) spectra at the D_2O–DPTAP interface. For D_2O, the bending mode is shifted to ~1200 cm^{-1}, outside the studied frequency window, so that these measurements serve as a reference. For all the salt concentrations, the spectra commonly show a large positive peak at ~1720 cm^{-1} and a relatively small negative peak at ~1740 cm^{-1}. These peaks are attributed to the C=O stretch mode.[51] A striking change of the spectra with increasing salt concentration is the elevation of the baseline (frequency-independent nonresonant contribution). We then turn our

Figure 3. (a,b) The $\Delta\text{Im}(\chi_{\text{eff}}^{(2)}(\omega,c))$ spectra obtained through the subtraction of D_2O data from the H_2O data of the (a) DPTAP and (b) DPPG samples at two different salt concentrations. The spectra are offset by 0.01 for clarity. (c,d) The $\Delta\Delta\text{Im}(\chi_{\text{eff}}^{(2)}(\omega))$ spectra for the (c) DPTAP and (d) DPPG interfaces obtained through the subtraction of $\Delta\text{Im}(\chi_{\text{eff}}^{(2)}(\omega,c = 1M)$ spectrum from $\Delta\text{Im}(\chi_{\text{eff}}^{(2)}(\omega,c = 0.1\ M)$ spectrum. The features appearing in the region shaded in light blue result from the residual C=O contributions. The dotted lines indicate the residual nonresonant contribution inferred from the fits.

focus to the $\text{Im}(\chi_{\text{eff}}^{(2)})$ spectra of the H_2O−DPTAP samples. Here, the H−O−H bending mode appears as a 1650 cm^{-1} peak feature.[26,28] Upon increasing the salt concentration from 0.1 mM to 1 M, the 1650 cm^{-1} peak varies substantially.

Subsequently, we measured the $\chi_{\text{eff}}^{(2)}$ spectra of the H_2O- and D_2O-negatively charged DPPG samples. The spectra are shown in Figure 2. The D_2O−DPPG samples also show the positive 1720 cm^{-1} and negative 1740 cm^{-1} C=O stretch features, while the H_2O−DPPG samples possess the ∼1650 cm^{-1} H−O−H bending mode contribution, in addition to the C=O stretch features. Again, upon changing the salt concentration, the 1650 cm^{-1} peak varies.

The SFG response of the H_2O and D_2O samples in the measured frequency range can be approximated by

$$\chi_{\text{eff},H_2O}^{(2)}(\omega) = \chi_{H_2O}^{(2),\text{NR}} + \chi_{C=O,H_2O}^{(2),\text{R}}(\omega) + \chi_{\text{bend}}^{(2),\text{R}}(\omega)$$
$$+ \chi_{\text{bend}}^{(3),\text{R}}(\omega)\Phi(c)\frac{\kappa(c)}{\kappa(c) - i\Delta k_z} \quad (1)$$

$$\chi_{\text{eff},D_2O}^{(2)}(\omega) = \chi_{D_2O}^{(2),\text{NR}} + \chi_{C=O,D_2O}^{(2),\text{R}}(\omega) \quad (2)$$

respectively, where $\chi^{(2),\text{NR}}$ represents the nonresonant contribution, $\chi_{C=O}^{(2),\text{R}}(\omega)$ denotes the resonant contribution from the C=O stretch mode. c, Φ, κ, and Δk_z denote ion concentration, the surface potential, the inverse of the Debye length, and the mismatch of the wave-vectors along the surface normal in the reflected SFG configuration, respectively.[26,38] By assuming that $\chi_{H_2O}^{(2),\text{NR}}(\omega) = \chi_{D_2O}^{(2),\text{NR}}(\omega)$ and $\chi_{C=O,H_2O}^{(2),\text{R}}(\omega) = \chi_{C=O,D_2O}^{(2),\text{R}}(\omega)$, that is, the nuclear quantum effects (NQEs) are
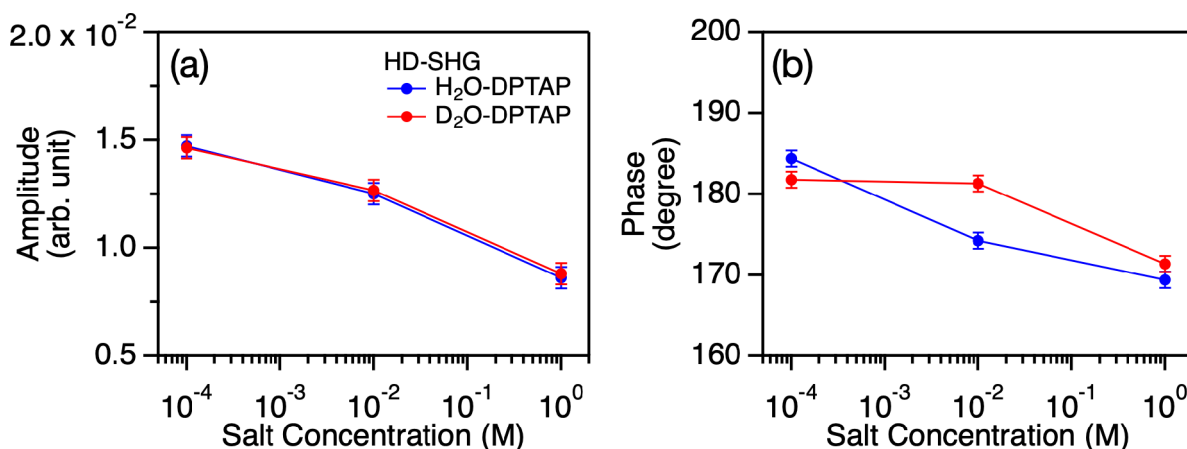
negligible, one can get the H−O−H bending mode contribution

$$\chi_{\text{bend}}^{(2),\text{R}}(\omega) + \chi_{\text{bend}}^{(3),\text{R}}(\omega)\Phi(c)\frac{\kappa(c)}{\kappa(c) - i\Delta k_z}$$

by subtracting $\chi_{\text{eff},D_2O}^{(2)}(\omega)$ from $\chi_{\text{eff},H_2O}^{(2)}(\omega)$. Here, we assumed negligible NQEs on the spectral shape, in analogy with previous work.[28] We will discuss the validity of this assumption in the following.

Figure 3 panels a and b show the subtracted spectra $(\Delta\text{Im}(\chi_{\text{eff}}^{(2)}(\omega,c)) = \text{Im}(\chi_{\text{eff},H_2O}^{(2)}(\omega,c)) - \text{Im}(\chi_{\text{eff},D_2O}^{(2)}(\omega,c)))$ of the DPTAP and DPPG samples, respectively. The $\Delta\text{Im}(\chi_{\text{eff}}^{(2)}(\omega,c))$ response in the 1580−1630 cm^{-1} frequency region decreases for the DPTAP sample, when the salt concentration increases from c = 0.1 mM to 1 M. On the other hand, the $\Delta\text{Im}(\chi_{\text{eff}}^{(2)}(\omega,c))$ response in the 1580−1630 cm^{-1} frequency region increases for the DPPG sample. The changes of the $\Delta\text{Im}(\chi_{\text{eff}}^{(2)}(\omega,c))$ spectra with varying salt concentration signify the non-negligible $\Delta\text{Im}(\chi_{\text{bend}}^{(3),\text{R}}(\omega))$ contribution.

We further calculated the spectra $\Delta\Delta\text{Im}(\chi_{\text{eff}}^{(2)}(\omega)) = \Delta\text{Im}(\chi_{\text{eff}}^{(2)}(\omega,c = 0.1\ \text{mM})) - \Delta\text{Im}(\chi_{\text{eff}}^{(2)}(\omega,c = 1\ \text{M}))$, which reflect the $\chi_{\text{bend}}^{(3),\text{R}}(\omega)\Phi(c)\frac{\kappa(c)}{\kappa(c) - i\Delta k_z}$ contribution (again under the assumption of negligible NQEs). The data are shown in Figure 3c,d for the DPTAP and DPPG samples, respectively. The $\Delta\Delta\text{Im}(\chi_{\text{eff}}^{(2)}(\omega))$ spectra showed a positive 1580−1670 cm^{-1} contribution for the DPTAP sample and a negative contribution for the DPPG sample. The $\Delta\Delta\text{Im}(\chi_{\text{eff}}^{(2)}(\omega))$ contribution in the ω < 1650 cm^{-1} region is more apparent than that in the ω > 1650 cm^{-1} region, where 1650 cm^{-1} is a typical H−O−H bending mode frequency. The prominent

Figure 4. (a,b) Amplitude (a) and phase (b) of the nonresonant contribution obtained by HD-SHG for water−DPTAP interface with various salt concentrations. The error bars indicate the 95% confidence intervals. The nonresonant contribution estimated from the fits of the HD-SFG data was also compared in the Supporting Information.

$\Delta\Delta\mathrm{Im}(\chi_{\mathrm{eff}}^{(2)}(\omega))$ contribution in the $\omega < 1650$ cm^{-1} region arises from the $\frac{\kappa(c)}{\kappa(c) - \Delta i k_z}$ term.

The positive and negative $\Delta\Delta\mathrm{Im}(\chi_{\mathrm{eff}}^{(2)}(\omega))$ contributions for the DPTAP and DPPG samples indicate that the $\Delta\Delta\mathrm{Im}(\chi_{\mathrm{eff}}^{(2)}(\omega))$ signal is governed by the

$$\mathrm{Im}\left(\chi_{\mathrm{bend}}^{(3),\mathrm{R}}(\omega)\Phi(c)\frac{\kappa(c)}{\kappa(c) - i\Delta k_z}\right)$$

term. Since the sign of the

$$\mathrm{Im}\left(\chi_{\mathrm{bend}}^{(3),\mathrm{R}}(\omega)\Phi(c)\frac{\kappa(c)}{\kappa(c) - i\Delta k_z}\right)$$

varies with the sign of the surface charge due to the surface potential of $\Phi(c)$, the flipping of the sign for $\Delta\Delta\mathrm{Im}(\chi_{\mathrm{eff}}^{(2)}(\omega))$ for the positively charged DPTAP and negatively charged DPPG surface provides direct evidence for the $\chi_{\mathrm{bend}}^{(3),\mathrm{R}}(\omega)$ contribution.

The current finding is at odds with that in ref 28 in which the H−O−H bending mode contribution is unchanged upon the addition of the salt. The reason for such a discrepancy may be attributable to the lipid monolayer formation. A lipid monolayer is easily displaced from the laser spot as a result of the heat accumulation due to continued laser irradiation.[43] Because we used the rotating trough, such heat accumulation can be avoided.
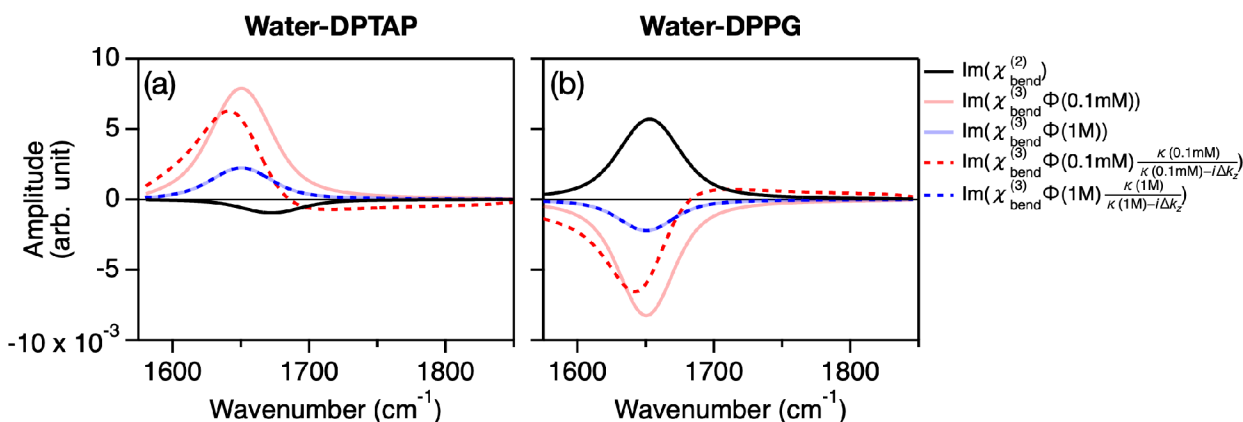
This hypothesis can be confirmed by investigating the SFG signature of the C=O stretch mode at the H$_2$O−DPTAP and D$_2$O−DPTAP interfaces. First, the ratio of the C=O stretch peak amplitude vs the H−O−H bending mode amplitude in the Im($\chi_{\mathrm{eff}}^{(2)}$) spectrum at the H$_2$O−DPTAP interface is much larger in this work than that reported in ref 28. This implies that the coverage of the DPTAP is higher in this work than in ref 28. Furthermore, the C=O peak frequency is ∼1730 cm^{-1} in the intensity $|\chi_{\mathrm{eff}}^{(2)}|^2$ spectra at the D$_2$O−DPTAP interface in refs 51 and 26, as well as our measurement (see Supporting Information), while the C=O peak is located at ∼1740 cm^{-1} in ref 28. Because the lower surface coverage of DPTAP results in the blue-shift of the C=O stretch peak,[51] the 1740 cm^{-1} C=O peak observed in ref 28 indicates that the coverage of the DPTAP is likely strongly reduced in the probed region. With decreasing surface coverage of DPTAP, the surface

charge decreases, lowering the impact of the $\chi_{\mathrm{bend}}^{(3)}$ contribution on the SFG spectra. Note that very recently, Bakker and co-workers also pointed out that too small a surface charge leads to negligibly small dipolar contribution of the bending mode in ref 44.

III.B. Determination of $\chi_{\mathrm{bend}}^{(2)}$ and $\chi_{\mathrm{bend}}^{(3)}$ Spectra. The above result of the significant $\chi_{\mathrm{bend}}^{(3)}$ contribution manifests that the $\chi_{\mathrm{bend}}^{(2)}$ and $\chi_{\mathrm{bend}}^{(3)}$ contributions are entangled in the measured $\chi_{\mathrm{eff}}^{(2)}$ spectra. Thus, disentangling the $\chi_{\mathrm{bend}}^{(2)}$ contribution from the $\chi_{\mathrm{bend}}^{(3)}$ contribution requires fitting of the spectra. Here, before carrying out the fitting, we verify the assumption that the NQE is negligible between the H$_2$O and D$_2$O samples. In fact, the different nonresonant background between the H$_2$O and D$_2$O samples can be seen in the nonzero ∼1800 cm^{-1} region of $\Delta\mathrm{Im}(\chi_{\mathrm{eff}}^{(2)}(\omega,c))$ of the DPTAP and DPPG samples as well as the SDS data in ref 28. Because the nonresonant contribution critically affects the inferred amplitude of the H−O−H bending mode signal, we checked whether the NQEs differentiate the nonresonant background of the H$_2$O and D$_2$O samples at the water−DPTAP interface by using HD-SHG spectroscopy. The amplitudes and phases obtained in the HD-SHG measurements are plotted in Figure 4 panels a and b, respectively, for DPTAP. The amplitude of the nonresonant contribution is very similar for the H$_2$O and D$_2$O samples, while the phase differs significantly, particularly for the 10 mM salt concentration. Currently, we are not sure how the NQEs affect the nonresonant contributions. Simulation techniques, including the NQEs,[52] may be able to clarify the origin of the difference between the H$_2$O and D$_2$O samples.

On the basis of the knowledge that the nonresonant contributions of the H$_2$O sample $\chi_{\mathrm{H_2O}}^{(2),\mathrm{NR}}$) and the D$_2$O sample ($\chi_{\mathrm{D_2O}}^{(2),\mathrm{NR}}$) can be different, we extracted the $\chi_{\mathrm{bend}}^{(2)}(\omega)$ and $\chi_{\mathrm{bend}}^{(3)}(\omega)$ contributions from the SFG spectra at the DPTAP and DPPG interfaces. For fitting the H−O−H bending mode contribution, we used a Voigt profile:[53,54]

$$\chi_{\mathrm{bend}}(\omega) = \frac{1}{\sqrt{2\pi}\Gamma_{\mathrm{bend,inh}}}\int_0^{\infty}\frac{A_{\mathrm{bend}}}{\omega_{\mathrm{bend}} - \omega' + i\Gamma_{\mathrm{bend,hom}}}$$
$$\exp\left(-\frac{(\omega - \omega')^2}{2\Gamma_{\mathrm{bend,inh}}^2}\right)\mathrm{d}\omega' \qquad (3)$$

Figure 5. (a,b) $Im(\chi_{bend}^{(2)}(\omega))$, $Im(\chi_{bend}^{(3)}(\omega)\Phi(c))$, and $Im(\chi_{bend}^{(3)}(\omega)\Phi(c)(\kappa(c)/(\kappa(c)-i\Delta k_z)))$ spectra obtained from the fit for (a) water-DPTAP and (b) water-DPPG interfaces, respectively. The $Im(\chi_{bend}^{(2)}(\omega))$ and $Im(\chi_{bend}^{(3)}(\omega)\Phi(c))/Im(\chi_{bend}^{(3)}(\omega)\Phi(c)(\kappa(c)/(\kappa(c)-i\Delta k_z)))$ contributions indicate the Stern layer contribution and the diffuse layer contribution, respectively. The $Im(\chi_{bend}^{(3)}(\omega)\Phi(c)(\kappa(c)/(\kappa(c)-i\Delta k_z)))$ contribution includes the phase mismatching term, showing the effective diffuse layer contribution in the $Im(\chi_{eff,H_2O}^{(2)}(\omega))$ spectra.

where A_{bend}, ω_{bend}, and $\Gamma_{bend,hom}$ denote, respectively, the amplitude, characteristic frequency, and line width associated with homogeneous broadening, and $\Gamma_{bend,inh}$ accounts for inhomogeneous broadening. For the fit of the C=O stretch modes, we used the two Lorentzian functions corresponding to the positive and negative features.[51]

We performed the global fitting for all 16 spectra (H_2O/D_2O × two different salt concentration × imaginary/real parts × DPTAP/DPPG). Here, $\chi_{bend}^{(3)}(\omega)$ was kept fixed across all eight H_2O spectra, because $\chi_{bend}^{(3)}(\omega)$ reflects the bulk water properties and should thus be independent of the lipid species. The four H_2O−DPTAP spectra and the four H_2O−DPPG spectra each had one fixed $\chi_{bend}^{(2)}(\omega)$ contribution is largely independent of the ionic strength and thus is insensitive to the salt concentration. Furthermore, the parameters for the C=O stretch modes were identical between H_2O and D_2O samples. The global fitting provides the robust estimation of the $\chi_{bend}^{(2)}(\omega)$ and $\chi_{bend}^{(3)}(\omega)$ contributions. The details of the fitting functions and obtained parameters can be found in the Supporting Information.

The obtained fits are plotted in the solid lines of Figures 1(c−f) and 2, while the $\chi_{bend}^{(2)}(\omega)$ and $\chi_{bend}^{(3)}(\omega)\Phi(c)$ spectra obtained from the fit are shown in Figure 5. The inferred $Im(\chi_{bend}^{(2)}(\omega))$ and $Im(\chi_{bend}^{(3)}(\omega)\Phi(c))$ spectra are negative and positive for the DPTAP samples, while these are positive and negative for the DPPG samples. The mechanism of the opposite sign of the $\chi_{bend}^{(2)}(\omega)$ and $\chi_{bend}^{(3)}(\omega)\Phi(c)$ contributions was previously explained using *ab initio* calculations.[26] The $\frac{\kappa(c)}{\kappa(c)-i\Delta k_z}$ term causes a line shape modulation of $Im(\chi_{bend}^{(3)}(\omega)\Phi(c))$ spectra in the low concentration regime (red dotted lines in Figure 5), giving rise to the low frequency contribution in the frequency region of less than ~1650 cm^{-1}, as discussed above. We would like to stress that the opposite signs of the $Im(\chi_{bend}^{(2)}(\omega))$ peak at the positively charged DPTAP and the negatively charged DPPG interfaces reveal that the H−O−H bending mode SFG feature arises from the dipole rather than from the quadrupole contribution.

The peak frequencies of the $\chi_{bend}^{(2)}(\omega)$ contribution at the H_2O−DPTAP and H_2O−DPPG interfaces were 1672 ± 10 and 1652 ± 2 cm^{-1}, respectively. Since a higher bending mode frequency indicates a stronger hydrogen bond,[1] the peak frequencies indicate that a water molecule in the vicinity of the

DPTAP interface has stronger hydrogen bonding than those at the DPPG interface. This trend is consistent with the O−H stretch data of the DPTAP and DPPG interface; the HD-SFG spectra show that the H_2O−DPTAP interface (center-of-mass frequency of 3360 cm^{-1}) shows a slightly lower frequency than the H_2O−DPPG interface (3390 cm^{-1}).[55] The slightly higher frequency of the H_2O molecules near the PO_4^- part of the phospholipid can be rationalized by previous simulation data.[56] This qualitative agreement between interfacial water stretch and bend frequencies substantiates the conclusion that the $\chi_{bend}^{(2)}(\omega)$ response originates from the interfacial dipole. As such, the $\chi_{bend}^{(2)}(\omega)$ peak contains information on the hydrogen bond structure of the interfacial water molecules.

The $\chi_{bend}^{(2)}(\omega)$ contribution has a peak frequency of 1650 cm^{-1} and a full-width at half-maximum (fwhm) of ~60 cm^{-1}. Since the $\chi_{bend}^{(3)}(\omega)$ contribution reflects the bulk properties, the peak frequency and fwhm of the $\chi_{bend}^{(3)}(\omega)$ spectra can be compared with the IR and Raman spectra of the water bending mode. Indeed, these values are very comparable to the 1644 cm^{-1} peak frequency and ~70 cm^{-1} fwhm of the IR spectrum of the water bending.[9]

IV. CONCLUSIONS

We performed the HD-SFG measurement of the H−O−H bending mode of water at the water-positively charged DPTAP and water-negatively charged DPPG interfaces. Our data show that the $\chi_{bend}^{(3)}(\omega)$ contributions are not negligible at the charged interface. The sign of the $Im(\chi_{bend}^{(2)}(\omega))$ spectrum at the water−DPTAP interface is negative, whereas the sign of the $Im(\chi_{bend}^{(2)}(\omega))$ spectrum at the water−DPPG interface is positive. The change of the peak sign indicates that the bending mode signal arises from the dipole mechanism. Furthermore, we discussed the obtained frequency for the $Im(\chi_{bend}^{(2)}(\omega))$. The sensitivity of the peak frequency at the different interfaces indicates that the bending mode of the interfacial water molecules can be a reporter for the hydrogen bonding structure at the interfaces.

■ ASSOCIATED CONTENT

ⓢ Supporting Information

The Supporting Information is available free of charge at https://pubs.acs.org/doi/10.1021/acs.jpcb.1c03258.

Further details for the experimental methods; discussion on frequency variations of the C≡O stretch mode between different research groups; fitting procedures; comparison of HD-SHG and HD-SFG data; phase-accuracy of HD-SFG measurements (PDF)

AUTHOR INFORMATION

Corresponding Author

Yuki Nagata − *Max Planck Institute for Polymer Research, 55128 Mainz, Germany;* orcid.org/0000-0001-9727-6641; Email: nagata@mpip-mainz.mpg.de

Authors

Takakazu Seki − *Max Planck Institute for Polymer Research, 55128 Mainz, Germany;* orcid.org/0000-0002-3999-2313

Chun-Chieh Yu − *Max Planck Institute for Polymer Research, 55128 Mainz, Germany*

Kuo-Yang Chiang − *Max Planck Institute for Polymer Research, 55128 Mainz, Germany;* orcid.org/0000-0001-5446-0270

Junjun Tan − *Hefei National Laboratory for Physical Sciences at the Microscale, and Department of Chemical Physics, University of Science and Technology of China, 230026 Hefei, China*

Shumei Sun − *Department of Physics and Applied Optics Beijing Area Major Laboratory, Beijing Normal University, Beijing 100875, China*

Shuji Ye − *Hefei National Laboratory for Physical Sciences at the Microscale, and Department of Chemical Physics, University of Science and Technology of China, 230026 Hefei, China;* orcid.org/0000-0002-3286-5258

Mischa Bonn − *Max Planck Institute for Polymer Research, 55128 Mainz, Germany;* orcid.org/0000-0001-6851-8453

Complete contact information is available at:
https://pubs.acs.org/10.1021/acs.jpcb.1c03258

Author Contributions

[#]T.S. and C.-C.Y. contributed equally.

Notes

The authors declare no competing financial interest.

REFERENCES

(1) Seki, T.; Chiang, K.-Y.; Yu, C.-C.; Yu, X.; Okuno, M.; Hunger, J.; Nagata, Y.; Bonn, M. The Bending Mode of Water: A Powerful Probe for Hydrogen Bond Structure of Aqueous Systems. *J. Phys. Chem. Lett.* **2020**, *11*, 8459−8469.

(2) Falk, M. The Frequency of the H-O-H Bending Fundamental in Solids and Liquids. *Spectrochim. Acta Part A Mol. Spectrosc.* **1984**, *40*, 43−48.

(3) Seki, T.; Yu, C.-C.; Yu, X.; Ohto, T.; Sun, S.; Meister, K.; Backus, E. H. G.; Bonn, M.; Nagata, Y. Decoding the Molecular Water Structure at Complex Interfaces through Surface-Specific Spectros-

copy of the Water Bending Mode. *Phys. Chem. Chem. Phys.* **2020**, *22*, 10934−10940.

(4) Calegari Andrade, M. F.; Ko, H. Y.; Car, R.; Selloni, A. Structure, Polarization, and Sum Frequency Generation Spectrum of Interfacial Water on Anatase TiO_2. *J. Phys. Chem. Lett.* **2018**, *9*, 6716−6721.

(5) Yang, N.; Duong, C. H.; Kelleher, P. J.; McCoy, A. B.; Johnson, M. A. Deconstructing Water's Diffuse OH Stretching Vibrational Spectrum with Cold Clusters. *Science* **2019**, *364*, 275−278.

(6) Mitra, S.; Yang, N.; McCaslin, L. M.; Gerber, R. B.; Johnson, M. A. Size-Dependent Onset of Nitric Acid Dissociation in Cs + · $(HNO_3)(H_2O)$ n = 0−11 Clusters at 20 K. *J. Phys. Chem. Lett.* **2021**, *12*, 3335−3342.

(7) Deng, G.-H.; Shen, Y.; Chen, H.; Chen, Y.; Jiang, B.; Wu, G.; Yang, X.; Yuan, K.; Zheng, J. Ordered-to-Disordered Transformation of Enhanced Water Structure on Hydrophobic Surfaces in Concentrated Alcohol-Water Solutions. *J. Phys. Chem. Lett.* **2019**, *10*, 7922−7928.

(8) Kuligiewicz, A.; Derkowski, A.; Szczerba, M.; Gionis, V.; Chryssikos, G. D. Revisiting the Infrared Spectrum of the Water-Smectite Interface. *Clays Clay Miner.* **2015**, *63*, 15−29.

(9) Yu, C.-C.; Chiang, K.-Y.; Okuno, M.; Seki, T.; Ohto, T.; Yu, X.; Korepanov, V.; Hamaguchi, H.; Bonn, M.; Hunger, J.; et al. Vibrational Couplings and Energy Transfer Pathways of Water's Bending Mode. *Nat. Commun.* **2020**, *11*, 5977.

(10) Perakis, F.; De Marco, L.; Shalit, A.; Tang, F.; Kann, Z. R.; Kühne, T. D.; Torre, R.; Bonn, M.; Nagata, Y. Vibrational Spectroscopy and Dynamics of Water. *Chem. Rev.* **2016**, *116*, 7590−7607.

(11) Woutersen, S.; Bakker, H. J. Resonant Intermolecular Transfer of Vibrational Energy in Liquid Water. *Nature* **1999**, *402*, 507−509.

(12) McGuire, J. A.; Shen, Y. R. Ultrafast Vibrational Dynamics at Water Interfaces. *Science* **2006**, *313*, 1945−1948.

(13) Zhang, Z.; Piatkowski, L.; Bakker, H. J.; Bonn, M. Ultrafast Vibrational Energy Transfer at the Water/Air Interface Revealed by Two-Dimensional Surface Vibrational Spectroscopy. *Nat. Chem.* **2011**, *3*, 888−893.

(14) Eftekhari-Bafrooei, A.; Borguet, E. Effect of Surface Charge on the Vibrational Dynamics of Interfacial Water. *J. Am. Chem. Soc.* **2009**, *131*, 12034−12035.

(15) Nihonyanagi, S.; Yamaguchi, S.; Tahara, T. Ultrafast Dynamics at Water Interfaces Studied by Vibrational Sum Frequency Generation Spectroscopy. *Chem. Rev.* **2017**, *117*, 10665−10693.

(16) Tan, J.; Zhang, J.; Li, C.; Luo, Y.; Ye, S. Ultrafast Energy Relaxation Dynamics of Amide I Vibrations Coupled with Protein-Bound Water Molecules. *Nat. Commun.* **2019**, *10*, 1010.

(17) Huse, N.; Ashihara, S.; Nibbering, E. T. J.; Elsaesser, T. Ultrafast Vibrational Relaxation of O-H Bending and Librational Excitations in Liquid H_2O. *Chem. Phys. Lett.* **2005**, *404*, 389−393.

(18) Chuntonov, L.; Kumar, R.; Kuroda, D. G. Non-Linear Infrared Spectroscopy of the Water Bending Mode: Direct Experimental Evidence of Hydration Shell Reorganization? *Phys. Chem. Chem. Phys.* **2014**, *16*, 13172−13181.

(19) Imoto, S.; Xantheas, S. S.; Saito, S. Ultrafast Dynamics of Liquid Water: Frequency Fluctuations of the OH Stretch and the HOH Bend. *J. Chem. Phys.* **2013**, *139*, 044503.

(20) van der Post, S. T.; Hsieh, C.-S.; Okuno, M.; Nagata, Y.; Bakker, H. J.; Bonn, M.; Hunger, J. Strong Frequency Dependence of Vibrational Relaxation in Bulk and Surface Water Reveals Sub-Picosecond Structural Heterogeneity. *Nat. Commun.* **2015**, *6*, 8384.

(21) Carpenter, W. B.; Fournier, J. A.; Biswas, R.; Voth, G. A.; Tokmakoff, A. Delocalization and Stretch-Bend Mixing of the HOH Bend in Liquid Water. *J. Chem. Phys.* **2017**, *147*, 084503.

(22) Vinaykin, M.; Benderskii, A. V. Vibrational Sum-Frequency Spectrum of the Water Bend at the Air/Water Interface. *J. Phys. Chem. Lett.* **2012**, *3*, 3348−3352.

(23) Nagata, Y.; Hsieh, C.-S.; Hasegawa, T.; Voll, J.; Backus, E. H. G.; Bonn, M. Water Bending Mode at the Water-Vapor Interface Probed by Sum-Frequency Generation Spectroscopy: A Combined

Molecular Dynamics Simulation and Experimental Study. *J. Phys. Chem. Lett.* **2013**, *4*, 1872−1877.

(24) Dutta, C.; Benderskii, A. V. On the Assignment of the Vibrational Spectrum of the Water Bend at the Air/Water Interface. *J. Phys. Chem. Lett.* **2017**, *8*, 801−804.

(25) Dutta, C.; Mammetkuliyev, M.; Benderskii, A. V. Re-Orientation of Water Molecules in Response to Surface Charge at Surfactant Interfaces. *J. Chem. Phys.* **2019**, *151*, 034703.

(26) Seki, T.; Sun, S.; Zhong, K.; Yu, C.; Machel, K.; Dreier, L. B.; Backus, E. H. G.; Bonn, M.; Nagata, Y. Unveiling Heterogeneity of Interfacial Water through the Water Bending Mode. *J. Phys. Chem. Lett.* **2019**, *10*, 6936−6941.

(27) Kundu, A.; Tanaka, S.; Ishiyama, T.; Ahmed, M.; Inoue, K.; Nihonyanagi, S.; Sawai, H.; Yamaguchi, S.; Morita, A.; Tahara, T. Bend Vibration of Surface Water Investigated by Heterodyne-Detected Sum Frequency Generation and Theoretical Study: Dominant Role of Quadrupole. *J. Phys. Chem. Lett.* **2016**, *7*, 2597−2601.

(28) Ahmed, M.; Nihonyanagi, S.; Kundu, A.; Yamaguchi, S.; Tahara, T. Resolving the Controversy over Dipole versus Quadrupole Mechanism of Bend Vibration of Water in Vibrational Sum Frequency Generation Spectra. *J. Phys. Chem. Lett.* **2020**, *11*, 9123−9130.

(29) Shen, Y. R. Basic Theory of Surface Sum-Frequency Generation. *J. Phys. Chem. C* **2012**, *116*, 15505−15509.

(30) Yamaguchi, S.; Shiratori, K.; Morita, A.; Tahara, T. Electric Quadrupole Contribution to the Nonresonant Background of Sum Frequency Generation at Air/Liquid Interfaces. *J. Chem. Phys.* **2011**, *134*, 184705.

(31) Ni, Y.; Skinner, J. L. IR and SFG Vibrational Spectroscopy of the Water Bend in the Bulk Liquid and at the Liquid-Vapor Interface, Respectively. *J. Chem. Phys.* **2015**, *143*, 014502.

(32) Moberg, D. R.; Straight, S. C.; Paesani, F. Temperature Dependence of the Air/Water Interface Revealed by Polarization Sensitive Sum-Frequency Generation Spectroscopy. *J. Phys. Chem. B* **2018**, *122*, 4356−4365.

(33) Khatib, R.; Sulpizi, M. Sum Frequency Generation Spectra from Velocity-Velocity Correlation Functions. *J. Phys. Chem. Lett.* **2017**, *8*, 1310−1314.

(34) Tang, F.; Ohto, T.; Sun, S.; Rouxel, J. R.; Imoto, S.; Backus, E. H. G.; Mukamel, S.; Bonn, M.; Nagata, Y. Molecular Structure and Modeling of Water-Air and Ice-Air Interfaces Monitored by Sum-Frequency Generation. *Chem. Rev.* **2020**, *120*, 3633−3667.

(35) Matsuzaki, K.; Nihonyanagi, S.; Yamaguchi, S.; Nagata, T.; Tahara, T. Vibrational Sum Frequency Generation by the Quadrupolar Mechanism at the Nonpolar Benzene/Air Interface. *J. Phys. Chem. Lett.* **2013**, *4*, 1654−1658.

(36) Matsuzaki, K.; Nihonyanagi, S.; Yamaguchi, S.; Nagata, T.; Tahara, T. Quadrupolar Mechanism for Vibrational Sum Frequency Generation at Air/Liquid Interfaces: Theory and Experiment. *J. Chem. Phys.* **2019**, *151*, 064701.

(37) Sun, S.; Schaefer, J.; Backus, E. H. G.; Bonn, M. How Surface-Specific Is 2nd-Order Non-Linear Spectroscopy? *J. Chem. Phys.* **2019**, *151*, 230901.

(38) Wen, Y.-C.; Zha, S.; Liu, X.; Yang, S.; Guo, P.; Shi, G.; Fang, H.; Shen, Y. R.; Tian, C. Unveiling Microscopic Structures of Charged Water Interfaces by Surface-Specific Vibrational Spectroscopy. *Phys. Rev. Lett.* **2016**, *116*, 016101.

(39) Gonella, G.; Lütgebaucks, C.; De Beer, A. G. F.; Roke, S. Second Harmonic and Sum-Frequency Generation from Aqueous Interfaces Is Modulated by Interference. *J. Phys. Chem. C* **2016**, *120*, 9165−9173.

(40) Ohno, P. E.; Saslow, S. A.; Wang, H.; Geiger, F. M.; Eisenthal, K. B. Phase-Referenced Nonlinear Spectroscopy of the α-Quartz/Water Interface. *Nat. Commun.* **2016**, *7*, 13587.

(41) Sung, W.; Seok, S.; Kim, D.; Tian, C. S.; Shen, Y. R. Sum-Frequency Spectroscopic Study of Langmuir Monolayers of Lipids Having Oppositely Charged Headgroups. *Langmuir* **2010**, *26*, 18266−18272.

(42) Liu, W.; Wang, Z.; Fu, L.; Leblanc, R. M.; Yan, E. C. Y. Lipid Compositions Modulate Fluidity and Stability of Bilayers: Characterization by Surface Pressure and Sum Frequency Generation Spectroscopy. *Langmuir* **2013**, *29*, 15022−15031.

(43) Backus, E. H. G.; Bonn, D.; Cantin, S.; Roke, S.; Bonn, M. Laser-Heating-Induced Displacement of Surfactants on the Water Surface. *J. Phys. Chem. B* **2012**, *116*, 2703−2712.

(44) Moll, C. J.; Versluis, J.; Bakker, H. J. Direct Evidence for a Surface and Bulk Specific Response in the Sum-Frequency Generation Spectrum of the Water Bend Vibration. Preprint *Res. Square* **2021**, DOI: 10.21203/rs.3.rs-198452/v1.

(45) Nihonyanagi, S.; Yamaguchi, S.; Tahara, T. Direct Evidence for Orientational Flip-Flop of Water Molecules at Charged Interfaces: A Heterodyne-Detected Vibrational Sum Frequency Generation Study. *J. Chem. Phys.* **2009**, *130*, 204704.

(46) Livingstone, R. A.; Nagata, Y.; Bonn, M.; Backus, E. H. G. Two Types of Water at the Water-Surfactant Interface Revealed by Time-Resolved Vibrational Spectroscopy. *J. Am. Chem. Soc.* **2015**, *137*, 14912−14919.

(47) Nihonyanagi, S.; Mondal, J. A.; Yamaguchi, S.; Tahara, T. Structure and Dynamics of Interfacial Water Studied by Heterodyne-Detected Vibrational Sum-Frequency Generation. *Annu. Rev. Phys. Chem.* **2013**, *64*, 579−603.

(48) Shen, Y. R. Phase-Sensitive Sum-Frequency Spectroscopy. *Annu. Rev. Phys. Chem.* **2013**, *64*, 129−150.

(49) Xu, B.; Wu, Y.; Sun, D.; Dai, H.-L.; Rao, Y. Stabilized Phase Detection of Heterodyne Sum Frequency Generation for Interfacial Studies. *Opt. Lett.* **2015**, *40*, 4472−4475.

(50) Wang, H.; Gao, T.; Xiong, W. Self-Phase-Stabilized Heterodyne Vibrational Sum Frequency Generation Microscopy. *ACS Photonics* **2017**, *4*, 1839−1845.

(51) Dreier, L. B.; Bonn, M.; Backus, E. H. G. Hydration and Orientation of Carbonyl Groups in Oppositely Charged Lipid Monolayers on Water. *J. Phys. Chem. B* **2019**, *123*, 1085−1089.

(52) Nagata, Y.; Pool, R. E.; Backus, E. H. G.; Bonn, M. Nuclear Quantum Effects Affect Bond Orientation of Water at the Water-Vapor Interface. *Phys. Rev. Lett.* **2012**, *109*, 226101.

(53) Velarde, L.; Wang, H.-F. Unified Treatment and Measurement of the Spectral Resolution and Temporal Effects in Frequency-Resolved Sum-Frequency Generation Vibrational Spectroscopy (SFG-VS). *Phys. Chem. Chem. Phys.* **2013**, *15*, 19970−19984.

(54) Chen, S.-L.; Fu, L.; Gan, W.; Wang, H.-F. Homogeneous and Inhomogeneous Broadenings and the Voigt Line Shapes in the Phase-Resolved and Intensity Sum-Frequency Generation Vibrational Spectroscopy. *J. Chem. Phys.* **2016**, *144*, 034704.

(55) Mondal, J. A.; Nihonyanagi, S.; Yamaguchi, S.; Tahara, T. Three Distinct Water Structures at a Zwitterionic Lipid/Water Interface Revealed by Heterodyne-Detected Vibrational Sum Frequency Generation. *J. Am. Chem. Soc.* **2012**, *134*, 7842−7850.

(56) Nagata, Y.; Mukamel, S. Vibrational Sum-Frequency Generation Spectroscopy at the Water/Lipid Interface: Molecular Dynamics Simulation Study. *J. Am. Chem. Soc.* **2010**, *132*, 6434−6442.